Dilute nitride saturable absorber mirrors for optical pulse generation

2004 J. Phys.: Condens. Matter 16 S3107

(http://iopscience.iop.org/0953-8984/16/31/008)

INSTITUTE OF PHYSICS PUBLISHING JOURNAL OF PHYSICS: CONDENSED MATTER

J. Phys.: Condens. Matter **16** (2004) S3107–S3120 PII: S0953-8984(04)76288-8

Dilute nitride saturable absorber mirrors for optical pulse generation

Oleg Okhotnikov and Markus Pessa[1]

Optoelectronics Research Centre, Tampere University of Technology, PO Box 692, 33101 Tampere, Finland

E-mail: markus.pessa@orc.tut.fi

Received 13 February 2004
Published 23 July 2004
Online at stacks.iop.org/JPhysCM/16/S3107
doi:10.1088/0953-8984/16/31/008

Abstract

GaAs-based dilute nitride semiconductor saturable absorber mirrors, SESAMs, have been developed and employed as cavity end mirrors of fibre lasers to produce ultra-short optical pulses over a wide spectral range. These devices are shown to be able to mode-lock diode-pumped erbium-doped and ytterbium-doped fibre lasers at around 1.55 and 1 μm, respectively, and produce reliable, self-starting picosecond pulse operation. The SESAM-equipped fibre lasers represent a promising route to designing a portable (sub-)picosecond light sources for low-cost maintenance turnkey operation for a variety of applications.

1. Introduction

The realization of high-performance vertical-cavity devices suffers from several technological problems. One of these problems is a lack of pairs of suitable semiconductors needed for the preparation of distributed Bragg reflectors (DBRs) of the vertical-cavity devices. InP-based heterostructures, which now dominate fibre optical telecommunications wavelengths at 1.3 and 1.55 μm, exhibit a low refractive index contrast, making it impossible to fabricate the DBR with a broad stop-band and nearly 100% reflectivity. Another problem is that InP-based alloys have relatively poor thermal conductivity [1–5].

Substitutionally random dilute nitride alloys, $Ga_xIn_{1-x}N_yAs_{1-y}$, pseudomorphically growable on GaAs substrates may challenge the InP technology [6–8]. GaAs, being cost-effective and robust with good thermal conductivity, allows for the growth of dilute nitride vertical-cavity surface-emitting lasers (VCSELs) and semiconductor saturable absorber mirrors (SESAMs) in a single growth run. GaInNAs at a dilute limit ($y \leqslant 2\%$) is a good material for the quantum wells of VCSELs and SESAMs at $\lambda \geqslant 1.3$ μm. The GaInNAs/GaAs interface has a large conduction band discontinuity, which offers excellent confinement of

[1] Author to whom any correspondence should be addressed.

electrons in the quantum wells, while the DBR of GaAs/Al(Ga)As exhibits a high reflectivity and broad bandwidth. When taken together, these features promise a great potential for GaInNAs/Ga(Al)As in optoelectronic applications [8–12], even though high-quality GaInNAs materials are hard to fabricate by any technique [13].

In this paper we discuss the preparation and performance characteristics of GaInNAs/GaAs quantum-well saturable absorbers and study their applicability as cavity end mirrors in mode-locked, ultra-fast, rare-earth-doped fibre lasers.

2. Generation of short pulses by fibre lasers

Generating short optical pulses has become an increasingly important technology for many applications: micro-machining, thin-film formation, laser cleaning, medicine and biology. Exciting results have been obtained with ultra-short pulses in the ablation of a variety of materials. Short pulses are also desired for surface patterning, due to their non-contact character, yielding a high spatial resolution because they minimize the heat-affected and shock-affected zones in the surrounding materials [14]. In particular, compact ultra-short-pulse fibre lasers at $\lambda \leqslant 1\ \mu$m are attractive alternatives to bulky solid-state lasers.

The traditional gain medium is an erbium-doped fibre ($\lambda \approx 1.55\ \mu$m), but using other rare-earth dopants significantly extends the achievable spectral range. For example, a continuous-wave (cw) tunable operation and mode-locked pulse operation for three-level transitions of Nd:glass have been demonstrated at around 0.91 μm [15–17], while ytterbium-doped fibre lasers and fibre amplifiers operate at somewhat longer wavelengths, $0.97\ \mu\text{m} \leqslant \lambda \leqslant 1.15\ \mu$m [18]. In particular, a Yb-doped fibre, with its broad gain bandwidth, high optical conversion efficiency and large saturation fluence, offers an almost ideal gain medium for generating and amplifying wavelength-tunable optical pulses. The Yb fibre laser at 0.977 μm may be used as a master source for frequency doubling to produce 0.488 μm, which is now produced from bulky and inefficient Ar-ion lasers.

The ultra-fast fibre lasers and solid-state lasers have benefitted from the recent development of non-linear mirrors, the SESAMs. These components are able to self-initiate and sustain mode-locking [19–21]. The mirror parameters, such as an absorption recovery time, saturation fluence and insertion loss, are controllable by proper device design, epitaxial growth and post-growth treatment. Using SESAMs as cavity end mirrors in fibre lasers yields compact, environmentally stable light sources that cover a wide spectral range and generate optical pulses with durations from picoseconds to femtoseconds.

The main difficulty in generating short pulses by Yb (and Nd) fibre lasers stems from a large normal material dispersion of silica at $\lambda \leqslant 1.1\ \mu$m. Although a waveguide dispersion mechanism can be used to balance the material dispersion at long wavelengths, $\lambda > 1.3\ \mu$m, the mechanism is not suitable for short wavelengths to cause overall anomalous dispersion. A photonic bandgap fibre would be an attractive solution for intracavity dispersion compensation at short wavelengths, if sufficiently low splice loss and back-reflection were achieved [22]. Dispersion compensation by intracavity prisms or grating pairs is another approach in an attempt to offset the material dispersion. Using prisms and grating pairs researchers have reached stretched-pulse or soliton pulse regimes [20, 21, 23]. Yet, a compact picosecond laser requires more efficient solutions. Gires–Tournois mirrors and chirped fibre Bragg gratings are interesting possibilities for generating anomalous dispersion in a compact form, but their practicalities are still to be evaluated. Negative dispersion produced by a Gires–Tournois interferometer (GTI) or chirped mirrors supplies sufficient compensation for solid-state lasers, balancing the dispersion of the laser rod, but for the fibre lasers with gain media typically about 1 m in length, short pulse operation requires the use of grating pairs [20, 21].

In the present paper we address an important issue of cavity dispersion in ultra-fast fibre lasers. The results show that the use of a properly designed saturable absorber makes the start-up of mode-locking quite insensitive to the overall cavity dispersion.

A SESAM with a large change (ΔR) in its non-linear reflectivity, as incident light intensity is varied, would facilitate self-starting mode-locking in a laser cavity with a large net normal dispersion [19, 20, 23–25], but on the down side increasing ΔR lowers the threshold for Q-switching instability [26, 27].

Recently, we have exploited the dispersive properties of resonant SESAMs to change the average cavity dispersion and forced the laser to operate in a stretched-pulse mode-locking regime or soliton-assisted regime at 1.55 μm [28, 29]. This GTI-type SESAM with negative group-velocity dispersion (GVD) was used for intracavity chirp compensation to produce high-energy transform-limited pulses without any external pulse compression. Another SESAM with positive GVD was studied for the stretched-pulse regime to avoid the use of a dispersion-compensating fibre, thus reducing the non-linear effects in the laser cavity. In the present paper, we demonstrate a resonant SESAM for $\lambda \approx 1$ μm with a strongly enhanced non-linear contrast and achieve self-starting continuous-wave (cw) mode-locking with picosecond pulse durations, even for a large cavity dispersion (typical of the Yb fibre laser). We show that near-resonant operation of the saturable absorber prevents the low-frequency Q-switching instability. We also show that anti-resonant absorbers with relatively small ΔR cannot start mode-locking without dispersion compensation by means of an additional intracavity dispersive delay line.

3. Preparation of SESAMs

The SESAMs were grown on n-type GaAs(001) substrates by solid-source molecular beam epitaxy (MBE). A *rf*-coupled plasma source was attached to the MBE reactor to produce reactive nitrogen atoms from N_2. The bottom DBR with the stop-band centred at $\lambda \approx 1.55$ μm consisted of 26 pairs of undoped GaAs ($\lambda/4n = 112$ nm) and AlAs (131 nm) layers, yielding a maximum $R \approx 99.8\%$. A 1λ absorber region was placed on top of the DBR. This region comprised a group of five compressively strained ($\Delta a/a \approx -2.2\%$) 6 nm-thick $Ga_{0.64}In_{0.36}N_{0.035}As_{0.965}$ quantum wells, centred at the anti-node of the optical field. Each quantum well was surrounded by 2 nm tensile-strained $GaN_{0.02}As_{0.98}$ layers ($\Delta a/a \sim +0.4\%$) for partial strain compensation. The quantum wells were separated by quantum barriers of GaAs, each 16 nm in thickness. The growth temperature was 600 °C for the DBR and 460 °C for the absorption region. Neither growth interruptions nor thermal annealing treatment were applied. Anti-resonance was obtained by leaving the front surface uncoated ($R \approx 30\%$) and having the AlAs/GaAs DBR at the bottom. A resonant SESAM was made by coating the device with a reflecting layer, which significantly increased the microcavity finesse and enhanced $\Delta R/R$ at near-resonance wavelengths, as shown below.

The structure of the 1 μm SESAM was similar to that of the 1.55 μm SESAM with marginal differences in quantum wells and DBRs. We were particularly interested in high-contrast resonant absorbers containing microcavities, designed to match incident light.

A useful feature of the 1 μm dilute nitride SESAM is that the recovery time can be controlled by epitaxial growth and thermal annealing [30], as opposed to a 1 μm nitrogen-free GaInAs SESAM, which needs post-growth ion implantation (yielding controllable results) or an exceptionally low growth temperature in the MBE process (yielding unpredictable results) to achieve the desired dynamic properties.

A low-intensity reflectivity spectrum under white light illumination and photoluminescence, launched from the quantum wells of a 1.55 μm SESAM, are shown in figure 1(a). The corresponding reflectivity spectrum of a 1 μm SESAM is given in figure 1(b).

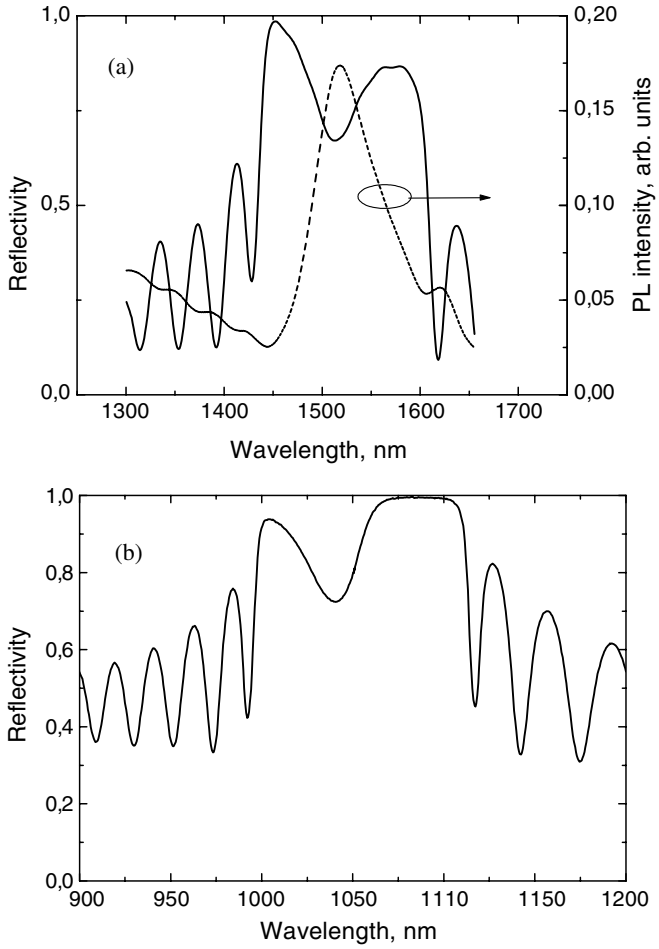

Figure 1. (a) Low-intensity reflectivity (full curve) and a photoluminescence spectrum (dotted curve) of the dilute nitride SESAM. Luminescence peak wavelength is 1.52 μm with FWHM of 89 nm. (b) Low-intensity reflectivity of a SESAM at about 1 μm.

4. Fibre lasers with dilute nitride saturable absorber mirrors operating in different spectral ranges

4.1. Long-wavelength erbium-doped fibre laser with a SESAM

Figure 2 shows the reflectivity of the 1.55 μm SESAM as a function of incident pulse energy. In this experiment we pumped the absorber with 1 ps pulses obtained from a tunable master-oscillator power-amplifier fibre source, butt-coupled with a SESAM. As the energy of the pump pulses was increased, ΔR increased non-linearly and reached a maximum value when the quantum wells were almost completely saturated at pump energies >100 pJ, giving rise to the modulation depth $\Delta R/R \approx 8\%$. The saturation fluence, $E_{\mathrm{sat,A}}$, was about 10 pJ cm^{-2}, deduced from the reflectivity change with the pulse energy.

The performance characteristics of the 1.55 μm SESAM as a mode-locking element were investigated in a linear cavity Er-doped fibre laser [28]. A Faraday rotator mirror was employed to compensate for environment-related polarization drifts in the cavity. It should be noted that

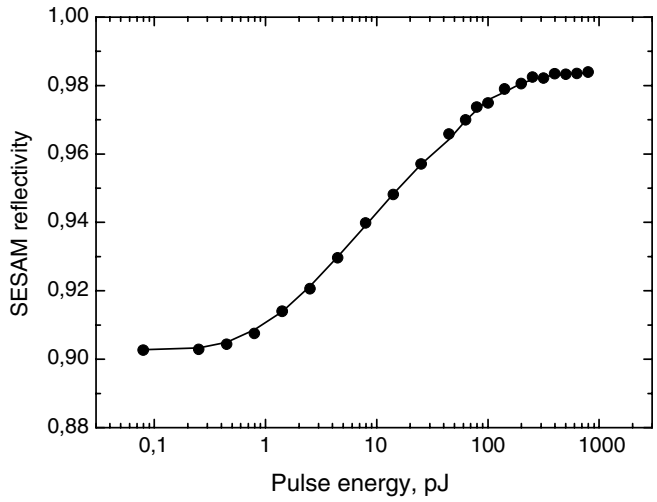

Figure 2. Measured change in SESAM reflectivity versus pulse energy.

the linear laser cavity represents a particular testbed for SESAMs because mode-locking in such a case is difficult to self-initiate, due to standing wave effects and spurious reflections. The fibre cavity, which was constructed of a Corning SMF28 fibre and a 2.2 m long Er fibre, had the fundamental repetition rate of 7 MHz. The cavity dispersion was dominated by the SMF28 fibre, ensuring operation in the anomalous dispersion (soliton) regime. The Er fibre had an un-pumped loss of 34 dB m^{-1} at 1.535 μm, a core diameter of 3.5 μm and a numerical aperture of 0.22. The laser was pumped with a single-mode semiconductor laser (120 mW at 0.98 μm), the output of which was taken *via* a 10% coupler. The fibre end was angle-cleaved to eliminate the influence of Fresnel reflection. The focal-spot diameter on the saturable absorber was 5–10 μm.

To demonstrate the broadband operation of a SESAM-equipped Er fibre laser, wavelength tuning was studied by inserting a bandpass filter with a 10 nm full width at half-maximum (FWHM) breadth. Figures 3(a) and (b) show background-free autocorrelation traces and optical spectra of the laser output, respectively. Without spectral filtering, the pulse width was 1.2 ps, assuming a sech^2 shape. The FWHM of the corresponding optical spectrum was 2.45 nm (figure 3(b)). Operating with anomalous cavity dispersion, solitonic sidebands emerge in the pulse spectrum. The corresponding time–bandwidth product was evaluated to be 0.36, which is close to the theoretical bandwidth limit. The tuning range over which self-starting mode-locking took place was about 30 nm, limited by the operational range of the dielectric filter used. The pulse widths changed from 1.28 to 1.58 ps for the whole tuning range, broadened with the filter; yet the temporal pulse profiles remained stable during tuning (figure 3(a)). The effect of filtering is evident from figure 3(b); spectral narrowing and soliton sideband suppression, due to filtering, can be clearly seen.

Figure 3(c) displays a stable mode-locked pulse train at the fundamental frequency (7 MHz). The average output power for the cw-mode-locked regime could be varied from 0.8 down to 0.03 mW. The threshold pump power was 30 mW.

4.2. Short-wavelength ytterbium-doped fibre laser with a SESAM

A SESAM with GaInNAs quantum wells can also be used to mode-lock lasers at 1 μm. We built an ytterbium-doped fibre laser operating at the blue edge of the gain spectrum. The

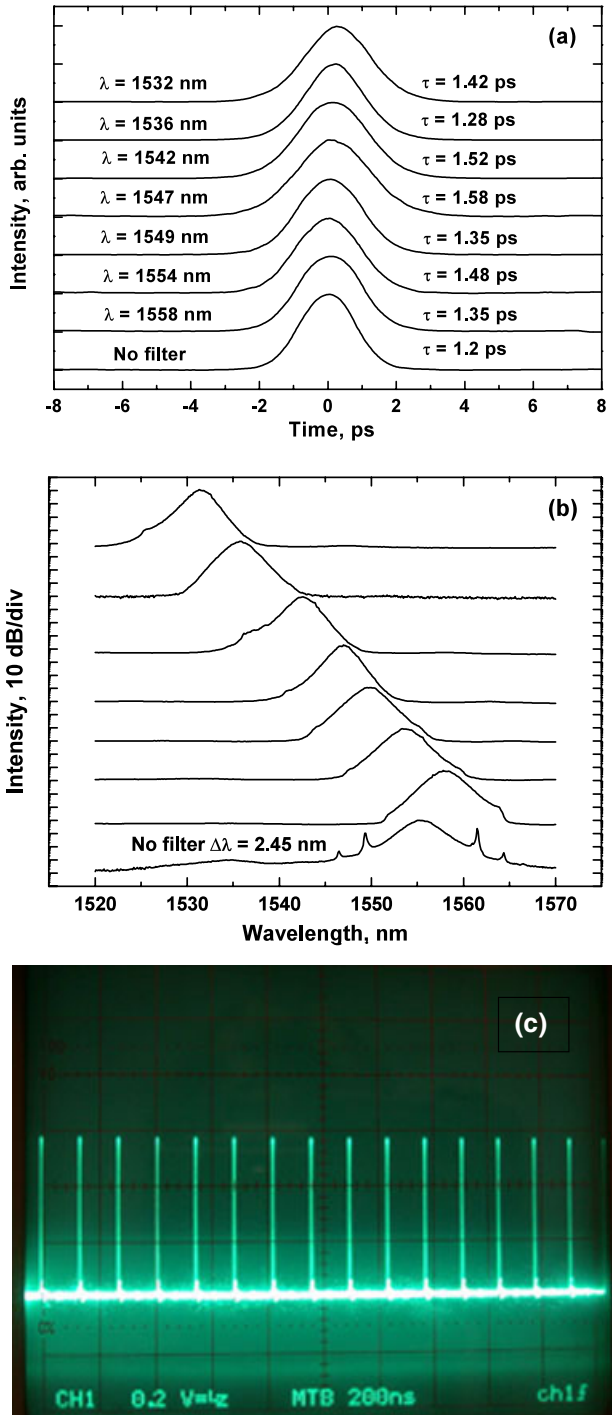

Figure 3. (a) Background-free autocorrelation traces of the mode-locked pulse trains for different central wavelengths. (b) Corresponding optical spectra and (c) the oscilloscope trace of the cw-mode-locked pulse train.

(This figure is in colour only in the electronic version)

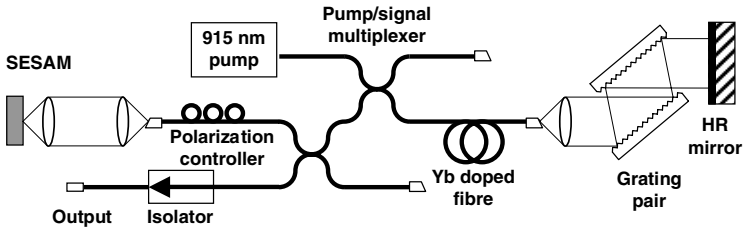

Figure 4. Cavity configuration for a 0.98 μm Yb-doped fibre laser.

schematic of a 0.98 μm mode-locked Yb-doped fibre laser with an integrated SESAM is shown in figure 4. The pump source (0.915 μm) was a single-mode fibre-pigtailed diode laser delivering up to 220 mW, taken through a 0.915/0.98 μm fused-fibre wavelength-dependent coupler. The absorber had $E_{\mathrm{sat,A}} \approx 3\ \mu\mathrm{J\ cm^{-2}}$ and $\Delta R/R \approx 12\%$.

The normal GVD of the fibre was compensated by anomalous dispersion of a grating pair (this SESAM was non-resonant, figure 4). The dispersion compensator comprised a gold-coated 1600 line $\mathrm{mm^{-1}}$ diffraction-grating pair. A high-R mirror (97% at 0.98 μm) and the SESAM formed the cavity ends. The output coupler had 7% transmission. Mode-locked operation was obtained for pump power levels above 40 mW and mode-locking was self-initiated at power levels above 50 mW. Figure 5(a) shows an autocorrelation trace and figure 5(b) shows a corresponding spectrum for the mode-locked pulse train with an output power of 3 mW, a repetition rate of 30 MHz and a pulse duration of 2.3 ps, resulting in an output pulse energy of 0.1 nJ. Absorbed pump power in the mode-locked regime was 25–30 mW. The laser threshold was around 20 mW.

The resultant 2.3 ps pulses were stable and nearly pedestal-free. These measurements were made for a grating separation of 6.5 cm, corresponding to a second-order dispersion of $-1.67\ \mathrm{ps^2}$ (double pass). The experimental autocorrelation trace (full curve, figure 5(a)) closely mimicked a Gaussian profile (dotted curve). The pulse spectrum (figure 5(b)) exhibited soliton sidebands (seen at all pump levels), implying that the laser operated in the anomalous-dispersion domain. The time–bandwidth product was 0.47, suggesting that the pulses were nearly bandwidth-limited with Gaussian temporal and spectral profiles. The average cavity dispersion was $-1.6\ \mathrm{ps^2}$, estimated from the soliton sidebands.

5. High-contrast resonant saturable absorber mirrors

5.1. Modelling of resonant SESAM

Theoretically, a high non-linear contrast of the cavity end mirror improves the self-starting capability of passive mode-locking. However, with an increase in mirror absorption the product of the saturation fluence of the absorbing material and non-linear contrast, $E_{\mathrm{sat,A}}\Delta R$, which determines the stability limit for cw-mode-locking, will also increase. This effect is not desired, since the stability condition (without solitonic effect) for cw-mode-locking against Q-switching requires [26]

$$E_{\mathrm{p}}^2 > E_{\mathrm{sat,L}} E_{\mathrm{sat,A}} \Delta R \tag{1}$$

on the assumption that the saturable absorber is fully saturated. Here, $E_{\mathrm{p}} = (P_{\mathrm{int}}/f_{\mathrm{rep}})$ is the intracavity energy and $E_{\mathrm{sat,L}}$ is the saturation energy of the gain (laser) medium; P_{int} is the intracavity average power and f_{rep} (= inverse round-trip time) is the pulse repetition rate.

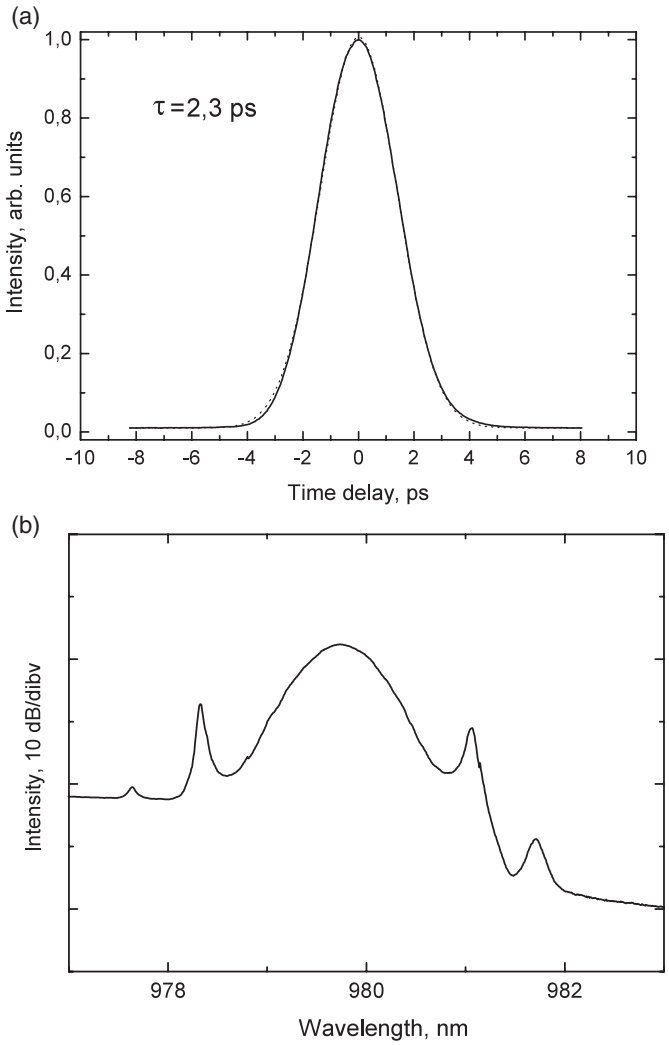

Figure 5. (a) Autocorrelation trace of generated pulses. (b) Measured optical spectrum (full curve), when the distance between gratings is 6.5 cm. The dotted curve shows a Gaussian fit.

An important observation is that ΔR can be increased by improving the SESAM cavity finesse by coating the device with a reflecting layer. The Fabry–Perot microcavity formed may or may not be in resonance with incident light. The analysis of such a SESAM reveals [24] that the effective saturation fluence of the entire mirror, $E^{\mathrm{eff}}_{\mathrm{sat,A}}$, decreases near the resonant wavelength with respect to $E_{\mathrm{sat,A}}$ of the 'non-cavity' SESAM, for which $E_{\mathrm{sat,A}}$ is solely determined by the material absorption. Therefore, $E^{\mathrm{eff}}_{\mathrm{sat,A}}$ strongly depends on cavity tuning/detuning conditions with respect to incident light. $E^{\mathrm{eff}}_{\mathrm{sat,A}}$ is related to $E_{\mathrm{sat,A}}$ of the absorption region *via* a multiplication factor η:

$$E^{\mathrm{eff}}_{\mathrm{sat,A}} = \eta E_{\mathrm{sat,A}} \tag{2}$$

where

$$\eta = \frac{1}{1-R_{\mathrm{T}}}\left[(1+\sqrt{R_{\mathrm{T}}R_{\mathrm{S}}})^2 - 4\sqrt{R_{\mathrm{T}}R_{\mathrm{S}}}\cos^2(\Phi_{rt}/2)\right]. \tag{3}$$

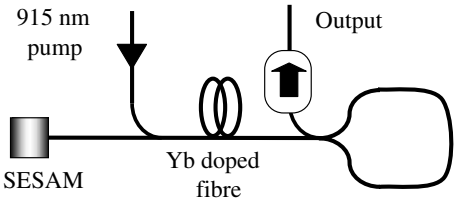

Figure 6. Schematic of a ytterbium fibre laser using a resonant saturable absorber mirror.

In equation (3), R_T is the reflectivity of the top mirror of the SESAM and Φ_{rt} is the amount of detuning. $R_S = R_B \exp(-4\alpha d)$ is the SESAM reflectivity ($R_B \approx 100\%$ for the bottom DBR) for an absorber with anti-reflection coating ($R_T \approx 0$). Hence $\eta \approx 1$. $\alpha(\lambda)$ is the absorption coefficient of the quantum-well region of thickness d. Then ΔR essentially depends on a change in R_S, resulting in

$$E^{\text{eff}}_{\text{sat,A}} \Delta R(\lambda) \approx E_{\text{sat,A}}[1 - R_S(\lambda)]. \tag{4}$$

Equation (4) determines the absorber contribution to the stability condition of equation (1). Because an increase in ΔR for near-resonance is compensated by a decrease in $E^{\text{eff}}_{\text{sat,A}}$, the product $E^{\text{eff}}_{\text{sat,A}} \Delta R(\lambda)$ remains constant around the resonant wavelength. As a consequence, using the resonant SESAM, both high ΔR and low $E^{\text{eff}}_{\text{sat,A}}$ can be obtained at the same time, which significantly improves self-starting mode-locking without violating equation (1) [26, 27].

5.2. Fibre laser at 1 μm *with a resonant SESAM*

A compact Yb-doped fibre laser exploiting a resonant absorber is shown in figure 6. The linear cavity contained a few centimetres long, heavily Yb^{3+}-doped fibre with an angle-cleaved end to suppress intracavity reflections, a wavelength-selective pump fibre combiner and a loop mirror ($R \approx 55\%$), which served as one of the cavity mirrors and an output coupler. Unsaturated absorption of this fibre was 500 dB m^{-1} at the diode-pump wavelength of 0.915 μm. A 0.915/1.05 μm pump/signal coupler and a loop mirror were made out of a fibre with a cut-off wavelength of 0.91 μm. The other end mirror was a resonant SESAM. A spectral filter was used occasionally in the fibre cavity to allow for tunable operation.

It was stated above that at the (near-)resonant wavelength the SESAM generates (small) anomalous dispersion, or normal dispersion, for blue or red detuning, respectively [23]. We obtained tunable mode-locking, independent of whether the dispersion of the SESAM was anomalous or normal, and no significant difference in operation was found. It was confirmed by calculations that the dispersion generated by the resonant SESAM was lower than the fibre dispersion so that the overall normal cavity dispersion was dominated by the fibre dispersion.

Figure 7 shows mode-locked spectra and low-intensity SESAM reflectivity near the resonant wavelength. Stable mode-locked operation was obtained for small wavelength detuning. For large detuning, i.e. for anti-resonant operation, cw-mode-locking was not achieved, and in the spectral ranges $\lambda < 1.03$ μm and $\lambda > 1.045$ μm only Q-switched mode-locking was observed. It should be noted that the stability condition (equation (1)) was preserved for all the detuning values studied. The Q-switched operation for large detuning was a clear indication of the non-self-starting character of mode-locking in this case. A typical autocorrelation trace (figure 8) corresponded to an 11 ps pulse (FWHM) with a Gaussian shape. The pulse repetition rates for all the laser configurations studied here ranged from 80 to 140 MHz.

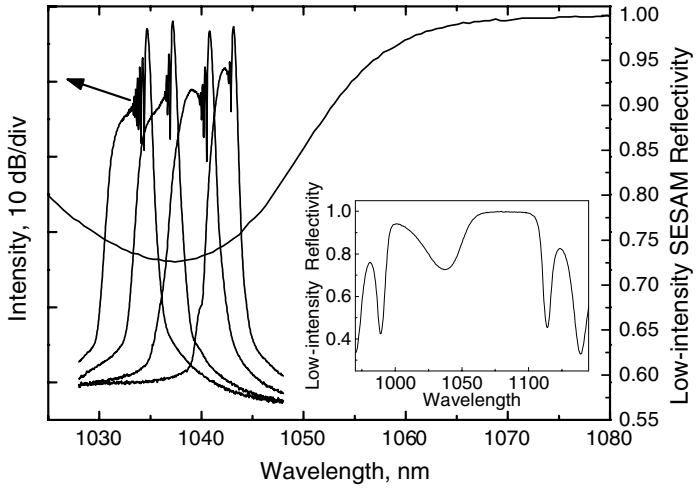

Figure 7. Pulse spectra achieved for cw-mode-locked operation by wavelength tuning using a spectral filter. Low-intensity reflectivity of the SESAM on a larger span is shown as an inset.

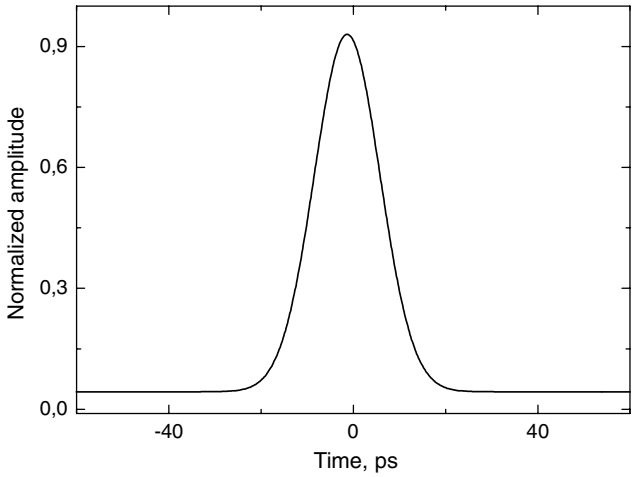

Figure 8. Typical autocorrelation obtained without dispersion compensation. The FWHM pulse width is 11 ps assuming a Gaussian pulse shape.

We found that non-linearity of the SESAM near resonance became very high and, in fact, dominated the non-linearity of the whole Yb laser with a sufficiently short cavity (for the short cavity, normal dispersion is reduced). This observation had an important consequence. It indicated that pulses could be solely shaped by the SESAM, which had slow-relaxation saturable non-linearity compared to an ultra-fast (Kerr) non-linearity of the fibre [31–34]. Remarkable asymmetry of the pulse spectrum, seen in figure 7, is more evidence resulting from a high nonlinear response of the resonant SESAM [32].

The above analysis confirms the dominant effect of the resonant SESAM on the start-up of cw-mode-locking at short wavelengths. To further explore this effect we calculated the number of cavity round-trips required to reach a steady-state cw-mode-locked operation for different ΔR values and, consequently, for different $E^{\mathrm{eff}}_{\mathrm{sat,A}}$. The laser was modelled by taking into account an output coupler, a dispersive element (e.g. a grating compressor, GTI), the active

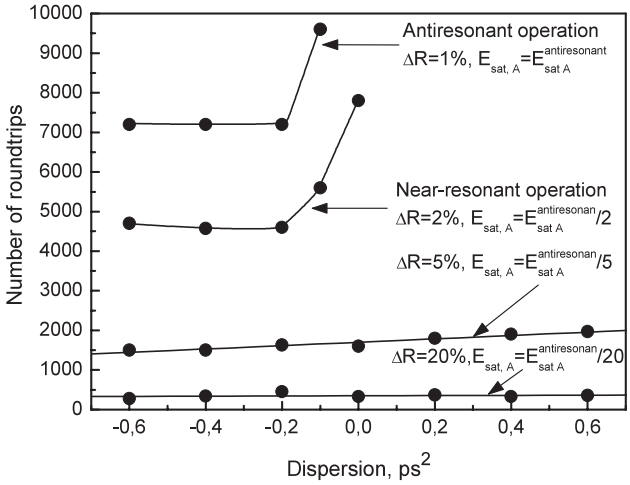

Figure 9. Results of numerical simulation representing the number of cavity round-trips necessary to achieve a steady-state operation for different non-linear contrasts ΔR of SESAM and for different values of net cavity dispersion.

and passive fibre segments of the cavity and a SESAM. The calculation included amplification, second-order dispersion and self-phase modulation. The propagation equation was solved by the split-step Fourier method [35]. The results are shown in figure 9. One can see that, for $\Delta R/R = 1\%$ (off-resonance), almost 10 000 round-trips are needed to achieve steady-state cw-mode-locking, while for $\Delta R/R = 20\%$ (near-resonance) less than 500 round-trips suffice.

The simulations revealed that, with a high-ΔR SESAM, the laser started mode-locking very efficiently and did so for a wide range of normal or anomalous dispersion values. In contrast, self-starting operation with a low-ΔR SESAM could only be achieved if the total cavity dispersion was small. Although the anomalous dispersion provides better conditions for self-starting mode-locking in general, it is obvious that the high non-linear response provided by the resonant SESAM is crucial for a reliable start-up without Q-switching instability.

Judging from the above analysis, one may conclude that $E^{\mathrm{eff}}_{\mathrm{sat,A}}$ increases significantly for large detuning, i.e. when the mirror operates at anti-resonance, tending to drive the transition from cw-mode-locking to Q-switched mode-locking. Experimentally, this effect is readily seen by measuring the spectra of a laser at various pump power levels. Figure 10 shows that with no filter in the laser cavity an increase in pump power, and therefore in pulse energy, red-shifted the mode-locked pulse spectra away from the 1.035 μm resonance point towards off-resonance wavelengths with higher saturation fluence $E^{\mathrm{eff}}_{\mathrm{sat,A}}$.

The output pulses were highly chirped in the laser with large normal dispersion. We compensated the chirp externally at the output of the laser using a grating pair. As a result, pulse durations as short as 6.8 ps were obtained for -5 ps^2 dispersion of the external delay line (figure 11), compared to a pulse duration of about 20 ps for uncompensated chirp.

The net positive dispersion of the Yb fibre was small, +0.0066 ps^2. This allowed dispersion compensation by a pair of intracavity prisms. Two SF 11 prisms were employed in our experiments. They provided an adjustable negative GVD. Figure 12 shows the pulse duration as a function of delay line dispersion. The minimum pulse duration achieved was 3 ps.

6. Conclusions

We have investigated dilute nitride quantum-well SESAMs, grown on standard GaAs(100) substrates by the MBE method, at the wavelengths of 1.55 and 1 μm and applied them as

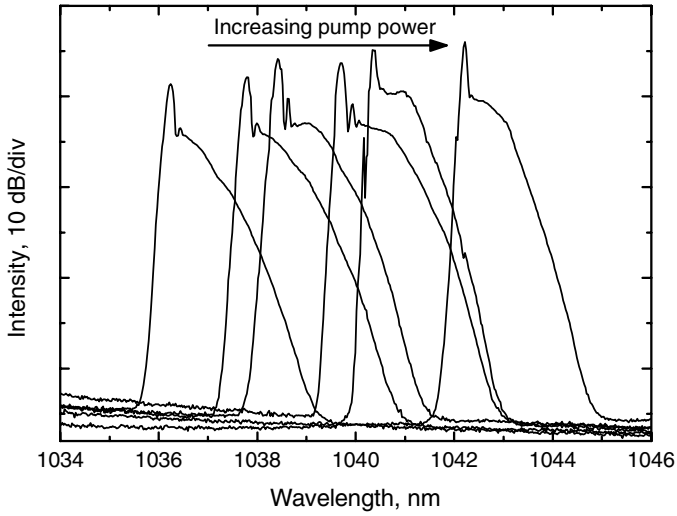

Figure 10. Evolution (progressive out of resonance shifting) of mode-locked spectra with an increase in the pump power. The SESAM resonant wavelength is positioned near 1035 nm.

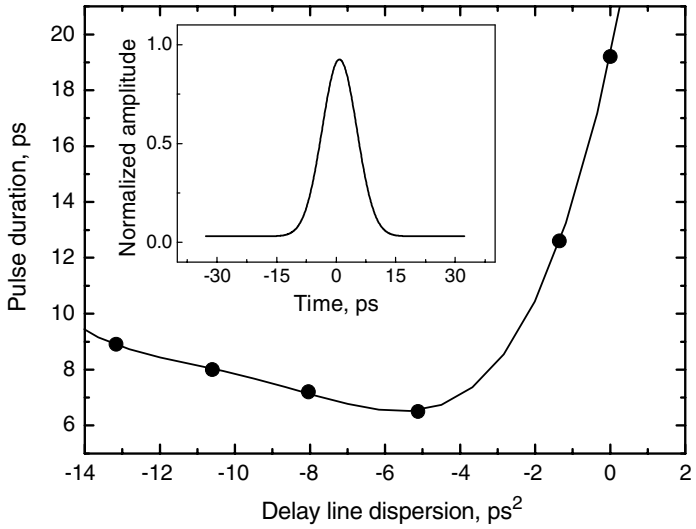

Figure 11. Pulse width versus external delay line dispersion. The inset shows the intensity autocorrelation of the shortest pulse obtained.

cavity end mirrors to passively mode-lock Er-doped and Yb-doped fibre lasers. Using the SESAM-equipped Er-doped laser we could generate 1.2 ps transform-limited pulses over the range from 1.53 to 1.56 μm. Using the SESAM-equipped Yb-doped laser at 1 μm, stable self-initiated mode-locking was achieved in a picosecond time regime. The difficulties in obtaining self-started mode-locking in the Yb laser, which exhibited a large net normal dispersion, were overcome by designing a resonant SESAM with a high non-linear contrast. It was found that a combined action of the fibre dispersion and non-linearity of the SESAM provided a pulse shaping mechanism. Consequently, the operation of a short-cavity Yb laser, having no

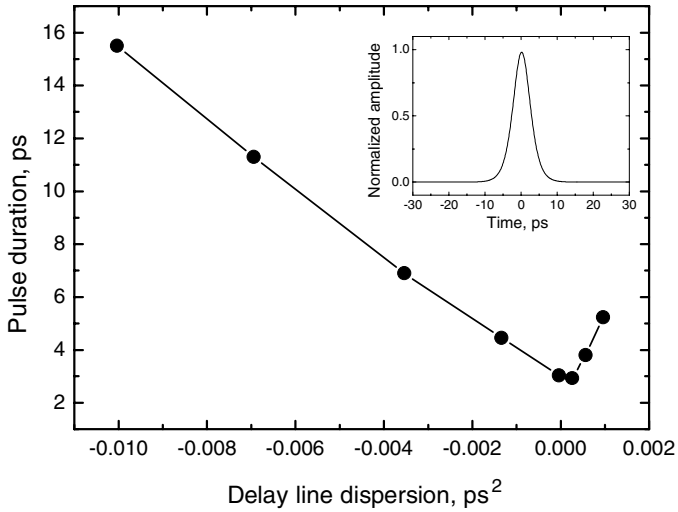

Figure 12. Pulse width versus net cavity dispersion obtained using a prism compensator. Intensity autocorrelation of the shortest pulse is shown as an inset.

dispersion-compensation schemes, could be perfectly stabilized against Q-switched mode-locking with the aid of the resonant SESAM.

Acknowledgments

The authors wish to thank students of the Optoelectronics Research Centre for their technical support and enthusiasm in carrying out research in this field. We are grateful to Dr A Grudinin, Fianium-NewOptics Ltd, UK, for many valuable discussions. The work was supported, in part, by the Technology Development Agency, Finland, within the ELMO TORCH Project and by the Academy of Finland within the TULE QUEST Project.

References

[1] Dia I F L, Nabet B, Kohl A, Benchimol J L and Harmand J C 1998 *IEEE Photon. Technol. Lett.* **10** 763
[2] Tai K, Fischer R J, Cho A Y and Huang K F 1989 *Electron. Lett.* **25** 1159
[3] Lambert B, Toudic Y, Rouillard Y, Gauneau M, Baude M, Alard F, Valiente I and Simon J C 1995 *Appl. Phys. Lett.* **66** 442
[4] Lambert B, Toudic Y, Rouillard Y, Baudet M, Guenais B, Deveaud B, Valiente I and Simon J C 1994 *Appl. Phys. Lett.* **64** 690
[5] Xiang N, Okhotnikov O, Vainionpää A, Guina M and Pessa M 2001 *Electron. Lett.* **37** 374
[6] Nakahara K, Kondow K, Kitatani T, Yazawa Y and Uomi K 1996 *Electron. Lett.* **32** 1585
[7] Riechert H, Egorov A Y, Bochert B and Illek S 2000 *Compound Semicond.* **6** 71
[8] Pessa M, Peng C S, Jouhti T, Pavelescu E-M, Li W, Karirinne S, Liu H and Okhotnikov O 2003 *IEE Proc.* J **150** 12
[9] Kondow M, Kitatani T, Nakatsuka S, Larson M C, Nakahara K, Yazawa Y, Okai M and Uomi K 1997 *IEEE J. Sel. Top. Quantum Electron.* **3** 719
[10] Ellmers C, Höhnsdorf F, Koch J, Agert C, Leu S, Karaiskaj D, Hofmann M, Stolz W and Rühle W W 1999 *Appl. Phys. Lett.* **74** 2271
[11] Choquette K D, Klem J F, Fischer A J, Blum O, Allerman A A, Fritz I J, Kurtz S R, Breiland W G, Sieg R, Geib K M, Scott J W and Naone R L 2000 *Electron. Lett.* **36** 1388
[12] Steinle G, Egorov A Y and Riechert H 2001 *Electron. Lett.* **37** 93

[13] Jouhti T, Peng C S, Pavelescu E-M, Konttinen J, Gomes L A, Okhotnikov O G and Pessa M 2002 *IEEE J. Sel. Top. Quantum Electron.* **8** 787
[14] Liu X, Du D and Mourou G 1997 *IEEE J. Quantum Electron.* **33** 1706
[15] Limpert J, Liem A, Schreiber T, Zellmer H and Tuennermann A 2003 *Electron. Lett.* **39** 645
[16] Hofer R, Hofer M, Reider G A, Cernusca M and Ober M H 1997 *Opt. Commun.* **140** 242
[17] Okhotnikov O G and Salcedo J R 1994 *Appl. Phys. Lett.* **64** 2619
[18] Zenteno L A, Minelly J D, Liu A, Ellison A J G, Crigler S G, Walton D T, Kuksenkov D V and Dejneka M J 2003 *Electron. Lett.* **37** 819
[19] Keller U, Weingarten K J, Kärtner F X, Kopf D, Braun B, Jung I D, Fluck R, Hönninger C, Matuschek N and Aus der Au J 1996 *IEEE J. Sel. Top. Quantum Electron.* **2** 435
[20] Okhotnikov O G, Jouhti T, Konttinen J, Karirinne S and Pessa M 2003 *Opt. Lett.* **28** 364
[21] Okhotnikov O G, Gomes L, Xiang N, Jouhti T and Grudinin A B 2003 *Opt. Lett.* **28** 1522
[22] de Matos C J S, Taylor J R, Hansen T P, Hansen K P and Broeng J 2003 *Opt. Express* **11** 2832
[23] Guina M, Xiang N and Okhotnikov O G 2002 *Appl. Phys.* B **74** S193
[24] Brovelli L R, Keller U and Chiu T H 1995 *J. Opt. Soc. Am.* B **12** 311
[25] Kärtner F X, Brovelli L R, Kopf D, Kamp M, Calasso I and Keller U 1995 *Opt. Eng. Bellingham* **34** 2024
[26] Hönninger C, Paschotta R, Morier-Genoud F, Moser M and Keller U 1999 *J. Opt. Soc. Am.* B **16** 46
[27] Haus H A 1976 *IEEE J. Quantum Electron.* **12** 169
[28] Okhotnikov O G and Guina M 2000 *Opt. Lett.* **25** 1624
[29] Guina M, Xiang N, Vainionpää A, Okhotnikov O G, Sajavaara T and Keinonen J 2001 *Opt. Lett.* **26** 1809
[30] Härkönen A, Jouhti T, Tkachenko N V, Lemmetyinen H, Ryvkin B, Okhotnikov O G, Sajavaara T and Keinonen J 2003 *Appl. Phys.* A **77** 861
[31] Kärtner F X, Aus der Au J and Keller U 1998 *IEEE J. Sel. Top. Quantum Electron.* **4** 159
[32] Gustafson T K, Taran J P, Haus H A, Lifsitz J R and Kelley P L 1969 *Phys. Rev.* **177** 306
[33] Paschotta R and Keller U 2001 *Appl. Phys.* B **73** 653
[34] Finlayson N, Wright E M and Stegeman G I 1990 *IEEE J. Quantum Electron.* **26** 770
[35] Agrawal G P 2001 *Non-Linear Fibre Optics* (London: Academic)